

Employing lidar to detail vegetation canopy architecture for prediction of aeolian transport

Joel B. Sankey,^{1,7} Darin J. Law,² David D. Breshears,³ Seth M. Munson,^{4,5} and Robert H. Webb⁶

Received 28 January 2013; revised 7 March 2013; accepted 11 March 2013; published 12 May 2013.

[1] The diverse and fundamental effects that aeolian processes have on the biosphere and geosphere are commonly generated by horizontal sediment transport at the land surface. However, predicting horizontal sediment transport depends on vegetation architecture, which is difficult to quantify in a rapid but accurate manner. We demonstrate an approach to measure vegetation canopy architecture at high resolution using lidar along a gradient of dryland sites ranging from 2% to 73% woody plant canopy cover. Lidar-derived canopy height, distance (gaps) between vegetation elements (e.g., trunks, limbs, leaves), and the distribution of gaps scaled by vegetation height were correlated with canopy cover and highlight potentially improved horizontal dust flux estimation than with cover alone. Employing lidar to estimate detailed vegetation canopy architecture offers promise for improved predictions of horizontal sediment transport across heterogeneous plant assemblages. **Citation:** Sankey, J. B., D. J. Law, D. D. Breshears, S. M. Munson, and R. H. Webb (2013), Employing lidar to detail vegetation canopy architecture for prediction of aeolian transport, *Geophys. Res. Lett.*, 40, 1724–1728, doi:10.1002/grl.50356.

1. Introduction

[2] Aeolian processes are fundamentally important sediment-transport mechanisms in the geosphere and biosphere [Ravi *et al.*, 2011] and are especially influential in water-limited environments, such as savannas and woodlands, where vegetation is often patchy with areas of plant cover interspersed within a soil matrix [Ursino and Rulli, 2010; D’Odorico *et al.*, 2011]. The spatial heterogeneity and

structure of semiarid vegetation canopies causes a much different below-canopy wind pattern than is typically measured above canopies, making it difficult to quantify below-canopy wind characteristics and associated aeolian sediment transport [Lee, 1991; Breshears *et al.*, 2009]. Aeolian transport starts via horizontal sediment flux at the land surface, which can contribute to desertification and land degradation through erosion, export, and depletion of mineral, nutrient, and organic components of the soil [Harper *et al.*, 2010; Li *et al.*, 2007]. Aeolian transport is also receiving increased attention due to its influence on climate, hydrology, energy balance [Mahowald *et al.*, 2010], and impact on human safety and health [Griffin *et al.*, 2001].

[3] Prediction of horizontal sediment transport requires understanding of vegetation architecture that produces variability in shear stress imparted on the soil surface by wind [Okin, 2008; Raupach *et al.*, 1993]. Vegetation architecture is difficult to quantify quickly and accurately in detail, particularly within spatially heterogeneous shrublands, savannas, and woodlands [Okin, 2008]. The canopy cover, structure, and intercanopy gaps are vegetation architecture components that are main determinants of surface roughness, shear-stress partitioning, and other factors that drive horizontal sediment transport and wind erosion [Raupach *et al.*, 1993; Okin, 2008]. Vegetation reduces wind velocity and subsequent detachment force. Intercanopy gaps are likely transport sources as wind speed is less impeded by vegetation roughness. The response of wind erosion to changes in vegetation cover, stature, and gaps can be complex in landscapes with patchy vegetation and is likely not linear [Breshears *et al.*, 2009; Field *et al.*, 2009].

[4] Models have been developed that incorporate estimates of the spatial arrangement of vegetation, soil erodibility, and wind characteristics into simulations of sediment transport [Raupach *et al.*, 1993; Okin, 2008]. In particular, rapidly characterizing the spatial arrangement of vegetation at high resolution and precision can be difficult with traditional field-based instruments and methods which are often unidirectional, along linear transects, with few samples and imprecise measurements to adequately estimate height and lateral dimensions of individual plants, spacing between individuals, and overall abundance of vegetation. Lateral cover of vegetation is one example of a commonly used measurement that scientists suggest inadequately characterizes spatial arrangement of vegetation for aeolian transport models [Raupach *et al.*, 1993; Okin, 2008; Li *et al.*, 2013]. Remote sensing methods that provide rapid measurements at high resolution can produce valuable information to parameterize aeolian simulation models [McGlynn and Okin, 2006]. Light detection and ranging (lidar) devices are one type of remote sensing that measures complex vegetation structure at very high

All supporting information may be found in the online version of this article.

¹Western Geographic Science Center, U.S. Geological Survey, Flagstaff, Arizona, USA.

²School of Natural Resources and the Environment, University of Arizona, Tucson, Arizona, USA.

³School of Natural Resources and the Environment, and Department of Ecology and Evolutionary Biology, University of Arizona, Tucson, Arizona, USA.

⁴Southwest Biological Science Center, U.S. Geological Survey, Moab, Utah, USA.

⁵Geosciences and Environmental Change Science Center, U.S. Geological Survey, Denver, Colorado, USA.

⁶National Research Program, U.S. Geological Survey, Tucson, Arizona, USA.

⁷Grand Canyon Monitoring and Research Center, U.S. Geological Survey, Flagstaff, Arizona, USA.

Corresponding author: J. B. Sankey, Grand Canyon Monitoring and Research Center, U.S. Geological Survey, 2255 N Gemini Dr., Building #4, Flagstaff, AZ, 86001, USA. (jsankey@usgs.gov)

©2013. American Geophysical Union. All Rights Reserved.
0094-8276/13/10.1002/grl.50356

spatial resolution [Eitel *et al.*, 2010; Keightley and Bawden, 2010], providing information on the areal extent, height, and distance between vegetation components (e.g., trunks, limbs, leaves) that obstruct wind.

[5] In this study, we used terrestrial (tripod-based) lidar to characterize vegetation canopy architecture and spacing across a gradient of canopy cover in a mesquite (*Prosopis velutina*) shrubland. The expansion of shrubs like mesquite is occurring in many arid and semiarid regions of the world due to interactions among climate, rising CO₂, and natural and anthropogenic disturbances [Archer, 1999]. Many of these water-limited regions are predicted to become more arid and increase in human population [Christensen *et al.*, 2007], which can further alter shrub abundance. Unfortunately, shrub reduction prescriptions such as mechanical, chemical, or fire removal [Whitson and Scifres, 1980] can increase wind erosion [Miller *et al.*, 2012]. Seasonal changes in leaf production of deciduous shrublands [Villegas *et al.*, 2010a, 2010b], influenced by factors such as precipitation, temperature, or herbivory, can also affect wind erosion. The combined effects of these ecosystem dynamics and management treatments might induce or maintain erosion and related desertification processes [Turnbull *et al.*, 2012; D’Odorico *et al.*, 2011]. Therefore, we wanted to examine the feasibility of using lidar to quickly and precisely characterize vegetation architecture and predicting aeolian transport as a function of lidar-derived vegetation characteristics.

[6] We used a gradient of mesquite canopy cover [Villegas *et al.*, 2010a, 2010b] to explore how changes in canopy gap size impact wind flow and aeolian processes that are highly scale-dependent [Okin *et al.*, 2006; Breshears *et al.*, 2009; Field *et al.*, 2009]. To determine the amount of aeolian sediment flux generated from each of these sites, we incorporated a new method for rapid assessment of vegetation gap sizes scaled by upwind vegetation height into a wind erosion model [Okin, 2008]. Our primary objectives were as follows: (1) to determine how lidar-derived vegetation gap size and height characteristics varied across a continuum of low-to-high woody canopy cover and (2) to evaluate the potential of incorporating lidar-derived scaled gap sizes for predicting reasonable estimates of sediment flux.

2. Materials and Methods

2.1. Study Gradient

[7] The study area is in the northern Sonoran Desert at the 21,500 ha Santa Rita Experimental Range (SRER; 31.79°N, 110.84°W), which is a long-term research facility administered by the University of Arizona [McClaran *et al.*, 2002]. The SRER is situated on a piedmont of the Santa Rita Mountains, with slopes ranging from 4% to 8% at ~1200 m elevation. Precipitation ranges from 270 to 440 mm yr⁻¹ across the SRER, and more than half of the annual rainfall occurs from July to September during the North American monsoon [McClaran *et al.*, 2002]. The study area is typical of a southwest U.S. savanna dominated by velvet mesquite (*Prosopis velutina*) in the canopy and a variety of perennial and annual grasses in the understory. The SRER has a history of year-round livestock grazing and seasonal rotation grazing on select pastures since 1972 (17.8–77.5 ha animal unit year⁻¹) [McClaran *et al.*, 2002]. For this study, we used six previously designated 50 m transects for our sites that differ in mean mesquite canopy cover [see Villegas *et al.*, 2010a,

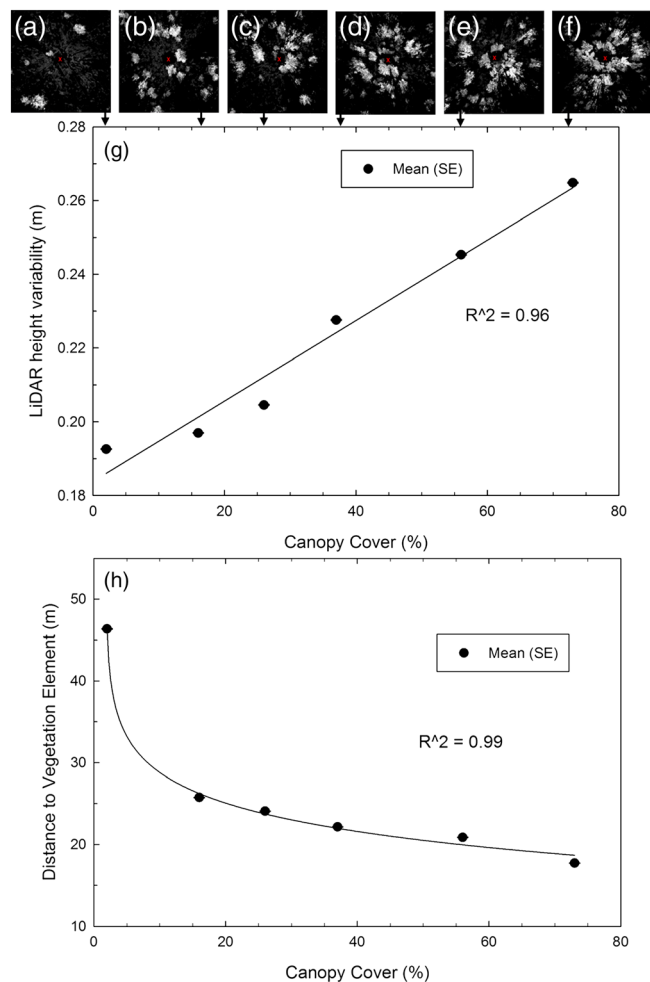


Figure 1. (a–f) Raster images of lidar height variability for the six transect locations (plan view, pixel brightness increases with increased height variability). (g) Mean lidar height variability versus canopy cover at the six mesquite transect locations. (h) Mean (SE) lidar distance to vegetation element (DTVE) versus canopy cover at the six mesquite transect locations.

2010b]. Therefore, the six transects represent a canopy-cover gradient (2%, 16%, 26%, 37%, 56%, 73%; measured from drip line to drip line down each transect). The transects were homogeneous with respect to soil, slope, aspect, elevation, and climate. The soil is weathered from Holocene-aged alluvium. Soil texture at the study area is sandy loam [Villegas *et al.*, 2010b], with a particle size distribution of sand (63 ± 14%), silt (16 ± 11%), and clay (21 ± 6%) [Field *et al.*, 2012].

2.2. Lidar

[8] We identified one point location from each transect to perform a lidar scan, such that the point had the same canopy cover (based on previous hemispherical photography estimates; Villegas *et al.* [2010b]) as the mean cover of the transect. For example, location 1 was a point with 2% cover on the first transect, and location 6 was a point with 73% cover on the sixth transect. We used an ILRIS 3D (OPTECH Inc., NY, USA) lidar instrument, mounted on a tripod from a scan position 1 m above ground and centered at each point

location with a plumb bob to measure a 360° horizontal view of the vegetation architecture at the six locations. The instrument employs a pulsed infrared (1535 nm) laser with a beam divergence of 0.00974° and beam diameter of 14 mm at a range of 50 m. Average (plan-view) point densities ranged from 66 to 293 points/cm² among the six data sets. Each of the six lidar point-cloud data sets was processed to determine the height variability and maximum height of lidar vegetation points at 0.1 m raster grid-cell size for a 100 m by 100 m extent using previously developed and described methods and lidar tools [http://bcal.geology.isu.edu/tools-2/envi-tools; *Streutker and Glenn*, 2006]. Lidar point-height variability was calculated as the standard deviation of all lidar point elevations (e.g., reflected from a plant) within the raster cell after the data were detrended to remove any effects of local topographic slope [http://bcal.geology.isu.edu/tools-2/envi-tools; *Streutker and Glenn*, 2006]. Lidar maximum vegetation height was calculated as the largest value of all lidar point elevations (e.g., reflected from a plant) within the raster cell [http://bcal.geology.isu.edu/tools-2/envi-tools]. Occluded pixels were recorded as no data. The rasterized data were analyzed to determine the horizontal distance from each location (i.e., the central point in each data set where the scanner was positioned) to each raster cell with a maximum height estimate and therefore surface roughness elements that might impede wind flow (e.g., leaves, branches, or trunks that reflected the laser pulses) in all directions, a variable we termed distance to vegetation element (DTVE) and which we used as an estimate of vegetation gap sizes. We scaled the DTVE for each raster cell by dividing by the maximum height value (henceforth “scaled gaps”) [*Okin*, 2008].

2.3. Horizontal Sediment-Transport Estimation

[9] We simulated total aeolian sediment flux for each point using a wind erosion model developed by *Okin* [2008]. This model accounts for variability in shear stress imparted on the soil surface as a function of the spatial arrangement of vegetation, with surfaces in the immediate wake of the plant receiving less shear stress than those farther away. The model uses a probability distribution function of the nearest upwind plant, scaled by plant height after user specification of the scaled vegetation gap size distribution and canopy cover. Additional inputs to run the model included wind speed distribution and threshold friction velocity of the bare soil surface. Details of the model and calibration are explained in *Okin* [2008] and *Munson et al.* [2011]. *Li et al.* [2013] further parameterized and validated the model using aeolian sediment traps distributed across rangelands in the western USA.

[10] For each of the six locations where lidar vegetation measurements were collected, we parameterized the model first with scaled vegetation gap size distribution from a histogram of the lidar-derived scaled gaps and second with the average scaled gap size estimated from belt transect (i.e., non-lidar) measurements of the spacing and heights of individual shrubs previously conducted by *Villegas et al.* [2010a, 2010b]. We used the canopy-cover estimates determined in the field for each sample location and a histogram of mean, 1 h windspeeds collected at 3 m height for September 2009 to April 2011 from the SRER weather station located adjacent to the transects (31.79°N, 110.84°W). We simulated sediment flux for a range of low, middle, and high values for threshold friction velocity of 0.24, 0.37, and 0.51 m s⁻¹. These threshold friction velocity values were selected as

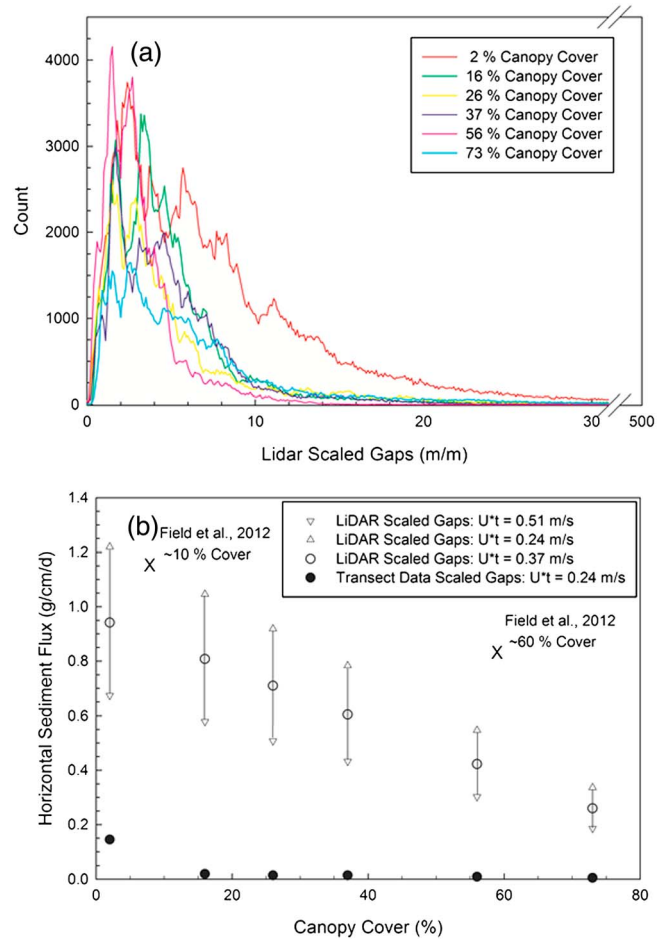


Figure 2. (a) Histograms of lidar-derived scaled gap values for the six transect locations. The histograms were used to parameterize vegetation scaled gap size distribution for *Okin's* [2008] wind erosion simulation model. (b) Total aeolian sediment flux at the six mesquite transect locations simulated with lidar-derived scaled gap size distributions or transect-based (non-lidar) measurements. Mean sediment-flux measurements by *Field et al.* [2012] of 1.16 and 0.84 g/cm/d (X's) from shrub patches of low (~10%) and high (~60%) vegetation cover, respectively, conducted during natural wind erosion events in this study environment are provided for reference.

representative for the range of particle diameters in sandy loam soils [*Shao and Lu*, 2000] and are reasonable for surfaces in this environment that generally do not have surface crusts and are often dry and loosely consolidated [*Field et al.*, 2012].

3. Results

[11] Raster images of lidar point-height variability illustrate the patchy (low and high amounts of cover) spatial pattern of mesquite vegetation (bright pixels in Figures 1a–1f) adjacent to sample locations. Lidar point-height variability was strongly and positively linearly correlated with the vegetation cover determined in the field (Figure 1g). The mean DTVE had a strong negative curvilinear relationship with increasing vegetation cover (Figure 1h). The average lidar gap size scaled by vegetation height was largest at the lowest cover (Figure 2a). Histograms of the abundance of points in lidar scaled gap size classes used to parameterize the sediment-

flux model illustrate how the distribution of scaled gaps varied among the locations with respect to canopy cover; in particular, a greater abundance of large scaled gaps is evident for lower canopy cover (Figure 2a).

[12] Total aeolian sediment flux modeled with lidar scaled gaps decreased linearly from $0.67 \text{ g cm}^{-1} \text{ d}^{-1}$ at the location with 2% canopy cover to $0.18 \text{ g cm}^{-1} \text{ d}^{-1}$ at the location with 73% canopy cover when threshold friction velocity was 0.51 m s^{-1} (Figure 2b). Total aeolian sediment flux modeled with lidar scaled gaps increased as threshold friction velocity decreased from 0.51 to 0.24 m s^{-1} . Fluxes determined from the transect (non-lidar) scaled gaps were 1–2 orders of magnitude less relative to fluxes determined with lidar scaled gaps (Figure 2b).

4. Discussion

[13] The presence, abundance, and canopy architecture of shrubby vegetation can vary dynamically over a range of spatial and temporal scales due to climatic and edaphic characteristics, disturbance, and management treatments. For example, leaf production varies over a seasonal to annual scale, whereas woody encroachment may occur over a decadal to centennial scale. Such dynamics are expected to create changes in canopy cover and gap sizes between vegetation canopies that could impact wind flow and sediment transport [Okin *et al.*, 2006; Breshears *et al.*, 2009; Field *et al.*, 2009]. We used lidar remote sensing and a gradient of shrub canopy cover to determine how lidar-derived vegetation gap size and height characteristics varied across a gradient of low-to-high canopy cover. Vegetation height variability increased linearly across the gradient of low-to-high canopy cover, whereas a curvilinear decrease was evident in the spacing (reflected in DTVE) between vegetation derived from lidar. There were nonlinear changes in vegetation gaps with respect to cover, such that decreases in gaps were larger at the low end of the cover gradient compared to the high end.

[14] Terrestrial (tripod-based) lidar produced rapid, higher resolution characterization of vegetation architecture and omnidirectional spacing than would typically be performed with field techniques. Terrestrial lidar can provide measurements at higher resolution and potentially lower cost, over smaller extent, relative to airborne lidar. While the terrestrial lidar approach is likely better suited to individual site (“spot”)–based measurements of scaled gaps, it could also have operational utility for evaluating the performance of airborne lidar or spectral imagery approaches that might be used to conduct analogous measurements over greater spatial extent. Terrestrial lidar therefore might offer an operationally unique and cost-effective approach relative to traditional field measurements and broad-scale airborne or spaceborne remote sensing.

[15] The incorporation of lidar-derived vegetation characteristics in model simulations of sediment fluxes resulted in flux estimates that were reasonable with respect to previously published flux measurements. Field *et al.* [2012] measured mean sediment fluxes of ~ 1.16 and $0.84 \text{ g cm}^{-1} \text{ d}^{-1}$ using sediment traps immediately downwind of shrub patches with ~ 10 and 60% shrub cover, respectively, in this same study area. These measurements are within the range of fluxes simulated with lidar scaled gaps from our study (0.2 – $1.2 \text{ g cm}^{-1} \text{ d}^{-1}$), although our flux estimates near 60% vegetation cover are ~ 30 – 60% smaller. Fluxes we simulated from more traditional,

non-lidar (transect-based) parameters were 1–2 orders of magnitude less than the Field *et al.* [2012] measurements at low and high vegetation cover. Field *et al.* [2012] measured fluxes for natural wind erosion events that occurred somewhat infrequently (at least four events per season) over short periods of time (hours) with minimum wind speeds of 4 m s^{-1} and gusts up to 13 m s^{-1} . Our examination of the feasibility of incorporating lidar-derived vegetation characteristics into the aeolian transport model simulated the average sediment flux from wind events that covered a comparable range in windspeed but were experienced at the site over a year. The longer time-integrated average estimate might contribute to some of the differences in simulated versus measured fluxes. Although the lidar metrics were very strongly related to woody canopy cover, additional discrepancy between simulated and measured fluxes might be influenced by herbaceous understory vegetation. Investigation of the extent that lidar can adequately account for separate effects of overstory and understory (woody and/or herbaceous) vegetation for characterization of scaled gaps and sediment-flux predictions might be important for further development of this approach.

[16] Simulated sediment transport across the gradient of canopy cover sheds light on how variability in vegetation cover across space and time can have a large effect on a major geomorphological process in dryland ecosystems. Results indicate that increases in vegetation element spacing (DTVE) as a result of decreased shrub canopy cover have the potential to be especially large at locations with relatively low shrub canopy cover. For temporally dynamic changes in vegetation cover, such as seasonal stages in leaf production (leaf-on, leaf-off) that occur during the year in deciduous (e.g., mesquite) shrublands, our results might suggest that the greatest annual variance in vegetation gap sizes and therefore sediment-transport potential occurs in locations of lower shrub cover, consistent with documented seasonal patterns of leaf phenology and associated changes in canopy structure [Villegas *et al.*, 2010b].

[17] Based on a previous synthesis, it has been suggested that disturbances that reduce vegetation cover might change the nature of the relationship between fluxes and cover [Breshears *et al.*, 2009]. While the data and model used in this study produced a linear relationship between flux and cover, our results suggest that a potentially large proportional increase in sediment transport could occur due to reduction in cover if coupled with an increase in soil erodibility (i.e., decrease in threshold friction velocity), particularly at locations of low shrub canopy cover (Figure 2b) [Li *et al.*, 2007]. Furthermore, climatic or land use effects may indirectly elicit nonlinear changes in flux through their impact on vegetation cover [Munson *et al.*, 2011]. Like many areas of the southwestern U.S., *Prosopis velutina* cover increased very rapidly in upland settings of the SRER at the beginning of the 20th century but showed an upper limit in cover later in the century due to density dependence and limits on water availability [Browning *et al.* 2008, Munson *et al.*, 2012]. Increased aridity predicted by climate change models will influence shrub abundances in the future and will interact with land use practices that can intensify changes in shrub abundance at a much shorter time scale. For example, management treatments that use the mechanical removal (cutting) of shrubs, or prescribed fire, to counter shrub expansion can limit shrub abundance. Although it may be more feasible to perform treatments in early successional

stages of encroachment where shrub cover is relatively low, our results suggest that the reduction of shrubs in conjunction with disturbances to the soil surface (e.g., increases in erodibility due to surface disturbance by humans and equipment) at these early stages of encroachment might especially exacerbate the erosion response after management [Li *et al.*, 2007; Field *et al.*, 2012; Miller *et al.*, 2012].

5. Conclusion

[18] This study highlights how the rapid characterization of vegetation architecture at high resolution using lidar remote sensing produced estimates of vegetation height and spacing that could be used to simulate reasonable estimates of aeolian fluxes when incorporated into a wind erosion model. Rapid and high-resolution characterization of vegetation architecture and incorporation into aeolian simulation models provides opportunities to evaluate aeolian processes relative to a wide variety of factors of contemporary importance in the geosphere and biosphere, including: increases in woody vegetation due to encroachment, decreases due to disturbance and management treatments, and interannual variability in deciduous vegetation cover due to climate seasonality and phenological events. The technique presented in this study and terrestrial lidar in general can be evaluated in terms of overall usefulness and cost-effectiveness relative to airborne lidar or spectral imagery over larger geographic extent in characterizing the spatial distribution of vegetation for aeolian models. Although we employed characterization of vegetation architecture to simulate aeolian processes, these techniques might have broader application for characterizing wind flow and aerodynamic parameters (irrespective of sediment transport) that have a wide range of biophysical relevance in environments with heterogeneous vegetation distribution such as for soil evaporation or partitioning of solar radiation.

[19] **Acknowledgments.** This research was supported by U.S. Geological Survey Mendenhall Fellowships (Joel Sankey and Seth Munson) and USGS Land Remote Sensing Program; additional support was provided by NSF Critical Zone Observatories (NSF EAR -0724958), NSF-DEB0816162, and Arizona Agricultural Experiment Station. We thank Greg Okin for help with the wind erosion model, Juan C. Villegas for field transect data, and Laura Norman and Dave Bedford for reviews. Mention of trade names or commercial products in this publication is solely for the purpose of providing specific information and does not imply recommendation or endorsement by the U.S. Geological Survey.

References

- Archer, S. (1999), Woody plant encroachment into southwestern grasslands and savannas: Rates, patterns and proximate causes, in *Ecological Implications of Livestock Herbivory in the West*, edited by M. Vavra, W. Laylock, R.D. Pieper, pp. 13–69, Society for Range Management, Denver, CO, USA.
- Breshears, D. D., J. J. Whicker, C. B. Zou, J. P. Field, and C. D. Allen (2009), A conceptual framework for dryland aeolian sediment transport along the grassland–forest continuum: Effects of woody plant canopy cover and disturbance, *Geomorphology*, *105*, 28–38.
- Browning, D. M., S. R. Archer, G. P. Asner, M. P. McClaran, and D. E. Wessman (2008), Woody plants in grasslands: Post-encroachment stand dynamics, *Ecol. Appl.*, *18*, 928–944.
- Christensen, J. H., et al. (2007), Regional climate projections, Climate Change, 2007: The physical science basis. Contribution of working group I to the fourth assessment report of the Intergovernmental Panel on Climate Change, University Press, Cambridge, Chapter 11, 847–940.
- D’Odorico, P., G. S. Okin, and B. T. Bestelmeyer (2011), A synthetic review of feedbacks and drivers of shrub encroachment in arid grasslands, *Ecohydrology*. doi:10.1002/eco.259.
- Eitel, J. U. H., L. A. Vierling, and D. S. Long (2010), Simultaneous measurements of plant structure and chlorophyll content in broadleaf saplings with a terrestrial laser scanner, *Remote Sens. Environ.*, *114*, 2229–2237.
- Field, J. P., J. Belnap, D. D. Breshears, J. C. Neff, G. S. Okin, J. J. Whicker, T. H. Painter, S. Ravi, M. C. Reheis, and R. L. Reynolds (2009), The ecology of dust, *Front. Ecol.* doi:10.1890/090050.
- Field, J. P., D. D. Breshears, J. J. Whicker, and C. B. Zou (2012), Sediment capture by vegetation patches: Implications for desertification and increased resource redistribution. *J. Geophys. Res.* *117*, G01033, doi:10.1029/2011JG001663.
- Griffin, D. W., C. A. Kellogg, and E. A. Shinn (2001), Dust in the wind: Long range transport of dust in the atmosphere and its implications for global public and ecosystem health, *Glob. Change Hum. Health*, *2*, 20–33.
- Harper, R. J., R. J. Gilkes, M. J. Hill, and D. J. Carter (2010), Wind erosion and soil carbon dynamics in south-western Australia, *J. Aeolian Res.*, *1*, 129–141.
- Keightley, K. E., and G. W. Bawden (2010), 3D volumetric modeling of grapevine biomass using Tripod LiDAR, *Comput. Electron. Agr.*, *74*, 305–312.
- Lee, J. (1991), Near-surface wind flow around desert shrubs, *Phys. Geogr.*, *12*, 140–146.
- Li, J., G. S. Okin, L. Alvarez, and H. Epstein (2007), Quantitative effects of vegetation cover on wind erosion and soil nutrient loss in a desert grassland of southern New Mexico, USA, *Biogeochem.*, *85*, 317–332.
- Li, J., G. S. Okin, J. E. Herrick, J. Belnap, M. E. Miller, K. Vest, and A. E. Draut (2013), Evaluation of a new model of aeolian transport in the presence of vegetation, *J. Geophys. Res.*, *118*, doi:10.1002/jgrf.20040.
- Mahowald, N. M., et al. (2010), Observed 20th century desert dust variability: Impact on climate and biogeochemistry, *Atm. Chem. and Phys.*, *10*, 10,875–10,893.
- McClaran, M. P., Angell, D. L., and C. Wissler (2002), Santa Rita Experimental Range Digital Database: User’s Guide. General Technical Report RM GTR-100. U.S. Department of Agriculture, Forest Service, Rocky Mountain Experiment Station, Ft. Collins, Colorado, USA.
- McGlynn, I. O., and G. S. Okin (2006), Characterization of shrub distribution using high spatial resolution remote sensing: Ecosystem implication for a former Chihuahuan Desert grassland, *Remote Sens. Environ.*, *101*, 554–566.
- Miller, M. E., M. A. Bowker, R. L. Reynolds, and H. L. Goldstein (2012), Post-fire land treatments and wind erosion—Lessons from the Milford Flat Fire, UT, USA, *J. Aeolian Res.*, *7*, 29–44.
- Munson, S. M., J. Belnap, and G. S. Okin (2011), Responses of wind erosion to climate-induced vegetation changes on the Colorado Plateau, *Proc. Nat. Acad. Sci.*, *108*, 3854–3859.
- Munson, S. M., R. H. Webb, J. Belnap, J. A. Hubbard, D. E. Swann, and S. Rutman (2012), Forecasting climate change impacts to plant community composition in the Sonoran Desert, *Glob. Change Biol.*, *18*, 1083–1095.
- Okin, G. S., D. A. Gillette, and J. E. Herrick (2006), Multi-scale controls on and consequences of aeolian processes in landscape change in arid and semi-arid environments, *J. Arid Environ.*, *65*, 253–275.
- Okin, G. S. (2008), A new model of wind erosion in the presence of vegetation. *J. Geophys. Res.* *113*, F02S10.
- Raupach, M. R., D. A. Gillette, and J. F. Leys (1993), The effect of roughness elements on wind erosion threshold, *J. Geophys. Res.*, *98*(D2), 3023–3029.
- Ravi, S., et al. (2011), Aeolian processes and the biosphere. *Rev. Geophys.* *49*, RG3001, doi:10.1029/2010RG000328.
- Shao, Y., and H. Lu (2000), A simple expression for wind erosion threshold friction velocity. *J. Geophys. Res.* *105*, D17.
- Streutker, D. E., and N. F. Glenn (2006), LiDAR measurement of sagebrush steppe vegetation heights, *Remote Sens. Environ.*, *102*, 135–145.
- Turnbull, L., B. Wilcox, S. Ravi, J. Belnap, G. S. Okin, K. Caylor, and T. E. Huxman (2012), The role of ecohydrological interactions and feedbacks on ecosystem state change, *Ecohydrology*. doi:10.1002/eco.265.
- Ursino, N., and M. C. Rulli (2010), Combined effect of fire and water scarcity on vegetation patterns in arid lands, *Ecol. Modell.*, *221*, 2353–2362.
- Villegas, J. C., D. D. Breshears, C. B. Zou, and P. D. Law (2010a), Ecohydrological controls of soil evaporation in deciduous drylands: How the hierarchical effects of litter, patch and vegetation mosaic cover interact with phenology and season, *J. Arid Environ.*, *74*, 595–602.
- Villegas, J. C., D. D. Breshears, C. B. Zou, and P. D. Royer (2010b), Seasonally pulsed heterogeneity in microclimate: Phenology and cover effects along deciduous grassland-forest continuum, *Vadose Zone J.* *9*, 537–547.
- Whitson R. E. and C. J. Scifres (1980), Economic comparisons of alternatives for improving honey mesquite-infested rangeland. Texas Agricultural Experiment Station Bull 1307. Texas A&M University, College Station, 185.